Global and Planetary Change 179 (2019) 10–22

Contents lists available at ScienceDirect

Global and Planetary Change

journal homepage: www.elsevier.com/locate/gloplacha

Holocene vegetation evolution and climatic dynamics inferred from an ombrotrophic peat sequence in the southern Altai Mountains within China

Wei Wang[a], Dongliang Zhang[b,c,*]

[a] School of Ecology and Environment, Inner Mongolia University, Hohhot 010021, China
[b] Xinjiang Institute of Ecology and Geography, Chinese Academy of Sciences, Urumqi 830011, China
[c] Research Central for Ecology and Environment of Central Asia, Chinese Academy of Sciences, 818 Beijing South Road, Urumqi 830011, China

ARTICLE INFO

Keywords:
Holocene climate change
Altai Mountains
Vegetation dynamics
Asian Arid Zone

ABSTRACT

Based on pollen data of 274 samples from a 550-cm core at Kelashazi Peat in the southern Altai Mountains within China, we reconstructed the Holocene vegetation dynamics and climatic change. The pollen assemblages and the associated biome scores indicate that the vegetation in Kelashazi valley was dominated by alpine meadows during the early Holocene (before ~8.2 cal. kyr BP) and by taiga forests in the middle Holocene (~8.2-~5.6 cal. kyr BP) that was followed by an expansion of alpine meadows (~5.6-~3.2 cal. kyr BP). The pollen-based temperature index-indicated thermal maximum lasting from ~8.0 to ~5.6 cal. kyr BP was consistent with temperature stack for 60–30°N and the later onset warming at Kelashazi Peat was associated with the cooling influence of remnant ice sheets in the early Holocene. The pollen-based increasing moisture index curve from Kelashazi Peat is in a good agreement with the synthesized decreasing aridity index curve in low-elevation regions of the Altai Mountains and the surrounding areas during the data-overlapping period between ~12.0 and ~3.2 cal. kyr BP. The Holocene wetting trend at Kelashazi Peat might have resulted not only from the increasing trend of NAO-related winter precipitation but also from the increasing trend of AMO-modulated summer precipitation.

1. Introduction

The Asian Arid Zone (AAZ) refers to the vast E-W striking arid belt that stretches from the Hinggan Mountains (~120°E) in the east to the Caspian Sea (~50°E) in the west. The core area of the Asian Arid Zone refers to the area around the Altai Mountains within the AAZ, including the eastern part of Kazakhstan, the Xinjiang area of China, the southern part of Russian Siberia and the western part of Mongolia. Within the core area the NW-SE striking Altai Mountains have been acknowledged as a conjunction between the westerly airflows from the west and the monsoon airflows from the east (Aizen et al., 2001; Chen et al., 2008, 2016; Feng et al., 2017; Ran and Feng, 2013; Rudaya et al., 2009; Xu et al., 2016). And, it might have also acted as a topographic barrier preventing the westerlies loaded with water vapor to enter the east and also preventing the monsoon-loaded water vapor to enter the west (Aizen et al., 2001; Chen et al., 2008; Harrison et al., 1996; Wang and Feng, 2013). This topographic barrier was widely reported to have resulted in a high-degree complexity of Holocene climate change in the core area (Aizen et al., 2001; Gong et al., 2001; Gong and Ho, 2002; Nagashima et al., 2011; Wang and Feng, 2013; Yang et al., 2019; Zhang and Feng, 2018).

The complexity can be illustrated by several competing propositions that are currently circulating to depict the proxy-recorded Holocene climate patterns. The first hypothesis argues for 'monsoon domination' in the core area, and the 'monsoon domination' is characterized by mega-humid early and middle Holocene climate (Cheng et al., 2012, 2016; Herzschuh, 2006; Li et al., 2011; Rudaya et al., 2009; Tarasov et al., 2000). The second hypothesis argues for 'westerly domination' in the core area, and 'westerly domination' is typified by a rather dry early Holocene and a quite humid middle and late Holocene (Chen et al., 2008). With an updated and expanded pollen dataset and more rigorous data quality screening, Wang and Feng (2013) demonstrated the Holocene climate has been persistently and slightly drying before the past ~8000 years in the northern Altai within the southern Russian Siberia and the slight drying trend was attributable to the decline of warm-season temperature that resulted in the decline of evaporation in the Atlantic Ocean. The same review (Wang and Feng, 2013) and two other reviews (Ran and Feng, 2013; Ran et al., 2015) all demonstrated that the northern Xinjiang area of northwestern China that includes the southern Altai has experienced a pronounced wetting trend during the

* Corresponding author at: Xinjiang Institute of Ecology and Geography, Chinese Academy of Sciences, Urumqi 830011, China.
E-mail address: zhdl@ms.xjb.ac.cn (D. Zhang).

https://doi.org/10.1016/j.gloplacha.2019.05.003
Received 18 November 2018; Received in revised form 2 May 2019; Accepted 2 May 2019
Available online 03 May 2019
0921-8181/ © 2019 Elsevier B.V. All rights reserved.

past ~8000 years and this wetting trend was more or less corroborated by several later works (e.g., Chen et al., 2016; Feng et al., 2017; Hong et al., 2014; Huang et al., 2018; Long et al., 2017; Mathis et al., 2014; Zhang et al., 2018a). Most recently, Zhang and Feng (2018), based on a thorough review of 30 published pollen sequences from the Altai Mountains and the surrounding areas, expanded the applicability of the '8000-year wetting trend' to the entire Holocene (i.e., past~11,500 years) and also to the entire Altai Mountains and the surrounding areas. The first-order variations (i.e., Holocene wetting trend) in the moisture level were proposed to have resulted from a combination of precipitation increasing and temperature decreasing, and the second-order variations superimposed on the first-order variations were speculated to have been associated with the IRD (ice-rafted debris)-suggested AMO (Atlantic Multidecadal Oscillation)-like events (i.e., Atlantic centennial oscillations).

To validate or invalidate the aforementioned propositions in portraying the temporal and spatial patterns, we retrieved a pollen sequence from a peat-lacustrine core (i.e., Kelashazi or KLSZ peat-lacustrine core) in Kelashazi Peat presently situated above the tree line in the southern Altai Mountains within China. We are dedicated to address following issues. First, what was the temporal pattern of the Holocene vegetation variations in the southern Altai Mountains? Second, what were the temporal patterns of the Holocene temperature and moisture changes in the southern Altai Mountains? Third, can a geographically coherent picture of climate change be more confidently depicted through a regional comparison of the published records?

2. Physiographic settings

The AAZ core area is presently under the influences of several climate systems. Specifically, the North Atlantic Oscillation (NAO) directs the tracks of the westerly jet (Aizen et al., 2001; Bridgman and Oliver, 2006; Meeker and Mayewski, 2002; Hurrell, 1996; Syed et al., 2006; Wirth et al., 2013) and affects the strength and position of the Siberian High Pressure system (Aizen et al., 2001; Bridgman and Oliver, 2006; Gong et al., 2001; Gong and Ho, 2002; Luo et al., 2016) during cold seasons, both (westerly jet and Siberian High) being significantly relevant to the climate in the core area (Fig. 1a). The East Asian summer monsoon (EASM) can bring precipitable water vapor to the eastern part of AAZ core area (Aizen et al., 2001; Meeker and Mayewski, 2002; Sun et al., 2015) (Fig. 1a). And, the eastward extension of the Azores High Pressure system can bring dry air masses to the western margin of the core area during warm seasons (Aizen et al., 2001; Bridgman and Oliver, 2006). In addition, frequent southward invasions of the polar front is of a great significance in generating precipitation in the core area during cold seasons (Zhang and Shi, 2002), and the North Pacific Ocean may be able to contribute a certain amount of precipitable water vapor to the core area under the positively-phased AMO conditions during warm seasons (Sun et al., 2015).

The NW-SE striking Altai Mountains in the center of the AAZ core area are documented to play an important role in shaping the modern bioclimatic patterns, and the Altai Mountains divide the core area into two parts: the western part and the eastern part. The western part is strongly influenced by the North Atlantic Ocean through westerly airflows (Chen et al., 2008; Ran and Feng, 2013; Wang and Feng, 2013) and the eastern part by the Pacific Ocean through Asian monsoonal airflows (Rudaya et al., 2009; Tarasov et al., 2000). The instrumental data show that the precipitation mainly occurs in summers in the eastern part and the precipitation seasonality (i.e., the difference between warm-season precipitation and cold-season precipitation) becomes less and less pronounced towards the west (Chen, 2010). The elevation-dependencies of the mean annual temperature (T_{ann}) and the mean annual precipitation (P_{ann}) in the Altai Mountains are rather pronounced (Chen, 2010). In addition, owing to the domination of the westerly airflows, the west-facing slopes (e.g., the Russian Altai with P_{ann} ~665 mm) receive more precipitation than the east-facing slopes (e.g., the Mongolian Altai with P_{ann} ~125 mm) in the Altai Mountains (Li, 1991; Zhang et al., 2018b).

The vegetation distributions closely follow the climate patterns. In the western part of the core area, dark taiga forests mainly consisting of spruce, larch and Siberian pine extensively develop in the elevations ranging from 1200 m a.s.l. to 2370 m a.s.l. And, the dark taiga forests gradually give way to larch-dominated light taiga forests southeastward, the latter (i.e., light taiga forests) being restricted to shady slopes at higher elevations ranging from 1700 to 2370 m a.s.l. in the eastern Altai Mountains (Hou, 2001). Further southeastward, the light taiga forests are replaced by alpine shrubs or/and meadows (Hou, 2001). In contrast, in the eastern part of the core area, only light taiga forest (i.e., pure larch) developed in the northern Altai Mountains (2100–2400 m a.s.l.), and this light taiga forest is replaced by alpine shrub or meadow towards the southeast (Hilbig, 1995; Lavrenko et al., 1979). It should be particularly noted that the alpine upper tree-line elevations in the western part (2330–2370 m a.s.l.) are approximately the same as those in the eastern part. But, the lower tree-line elevations differ greatly, being averagely 500 m lower in the western part than in the eastern part (Yuan, 1986).

Our study site, a lacustrine-peat core (48°07′N, 88°22′E, 2422 m a.s.l.) in Kelashazi Peat, is situated within the alpine meadow zone almost touching the alpine tree line in the southeastern Altai Mountains (Fig. 1b). The climate in the Kelashazi valley is sub-humid with a humidity index (i.e., ratio between the mean annual precipitation (MAP) and the potential evapotranspiration (ET_0)) of 0.80. Specifically, the MAP is 664 mm and the ET_0 is 838 mm with the mean annual temperature (MAT) of −3.6 °C at the nearby meteorological Sentasi station (48°10′N, 88°12′E, 2100 m a.s.l.). The area around Kelashazi valley is naturally landscaped with the following vegetation zones from higher to lower elevations (Fig. 2): snow patches and bare rocks above 3200 m a.s.l.; alpine tundra (mainly *Cetraria nivalis* mosses and lichens) between 3200 and 2800 m a.s.l.; alpine meadows (including *Kobresia* spp., *Carex* spp., *Festuca kryloviana*, *Alchemilla sibirica* and forbs) between 2800 and 2370 m a.s.l.; needle-leaved forests (mainly *Larix sibirica*) on shady slopes (i.e., north-facing and west-facing slopes) between 2370 and 1700 m a.s.l. and scrubs (including *Rosa sericea*, *Cotoneaster adpressus*) on sunny slopes (south-facing and east-facing slopes) between 2100 and 2370 m a.s.l. At lower elevations, subalpine meadows (mainly including *Calamagrostis epigejos* tall grass meadow, *Carex* spp., forbs meadow) develop between 1700 and 1300 m on shady slopes and between 1900 and 2100 m on sunny slopes; montane steppes (including *Festuca ovina*, *F. sulcata, Artemisia* spp.) occupy the area between 1300 and 800 m on shady slopes and between 1900 and 1200 m on sunny slopes. Towards the foothills of the mountains, desert steppes (mainly *A. boratalensis*, *Anabasia bravifolia*, *Nanophyton spp.*) develop extensively below 800 m a.s.l. on shady slopes and below 1300 m a.s.l. on sunny slopes (Hou, 2001; Yuan, 1986). The modern vegetation around the Kelashazi Peat (2422 m a.s.l.) is an alpine meadow (Abdusalih et al., 2008).

3. Materials and methods

3.1. Chrono-stratigraphy

A 550-cm-long peat-lacustrine core was obtained with a peat corer (BJ7R-0409) imported from Holland in 2013 in the lowest part of Kelashazi peat (Fig. 1c-d). Eleven peat samples (mostly *Sphagnum* stems) and three lake-mud bulk samples were radiocarbon dated using accelerator mass spectrometry (AMS) at the NSF-AMS Facility, University of Arizona (Table 1). Fig. 3 shows that twelve of the fourteen dates are in a good order and two dates (i.e., 8825 ^{14}C yr BP (8070 cal. yr BP) at depth of 460 cm and 9499 ^{14}C yr BP (9890 cal. yr BP) at depth of 350 cm) are off the order. The age-depth model (Fig. 3) was established by fitting spline functions to the age control points using the Clam library (Blaauw, 2010) with the INTCAL 09 calibration dataset

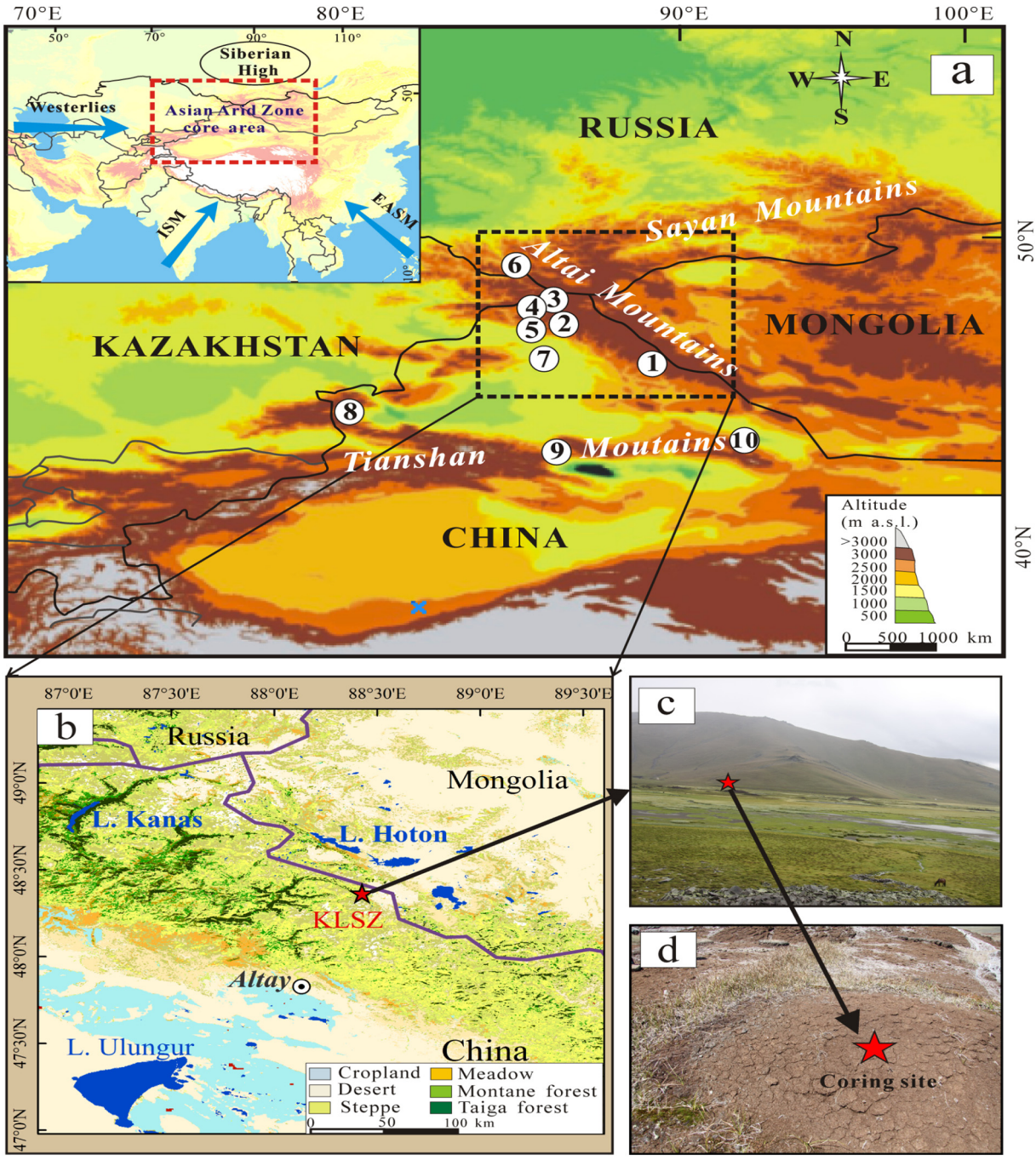

Fig. 1. Bioclimatic position of Kelashazi (KLSZ) lacustrine-peat core in the context of large-scale climate systems (a: upper panel) and in the context of the southern Altai vegetation (b: lower-left panel). Also included are the photos of Kelashazi valley (c) and the coring site (d). Sites referred in this study: (1) Kelashazi Peat (our studied site), (2) Kanas Lake, (3) Tielishahan Peat, (4) Habahe Peat, (5) Narenxia Peat, (6) Belukha ice core, (7) Wulungu Lake, (8) Sayram Lake, (9) Chaiwopu Peat, (10) Balikun Lake.

(Reimer et al., 2009). The bottom age of ~11,770 cal. yr BP and the surface age of ~3190 cal. yr BP were extrapolated on the basis of the age-depth model. The core can be stratigraphically divided into four units (Fig. 3). Unit 1 (550–515 cm; ~11,770-~11,220 cal. yr BP) is a lacustrine mud layer. Unit 2 (515–375 cm; ~11,224-~8770 cal. yr BP) is a strongly-decomposed peat layer. Unit 3 (375–150 cm; ~8770-~5610 cal. yr BP) is a moderately-decomposed peat layer. Unit 4 (150–0 cm; ~5610-~3190 cal. yr BP) is a poorly-decomposed peat layer.

3.2. Pollen analysis

Totally, 274 pollen samples were obtained at 2-cm intervals from the core. For pollen analysis, one tablet of *Lycopodium* (containing 27,637 ± 563 spores) was added for calculation of pollen concentration. The fossil pollen samples were treated with HCl (5–10%) and HF (36%) and sieved in ultrasonic bath with 7-μm cloth. Pollen types were identified using pollen references including pollen photographs (Wang et al., 1995) and our own type-slide collection. The treated samples were mounted and examined with a transmitted light microscope at 400× magnification. > 500 terrestrial pollen grains (not including

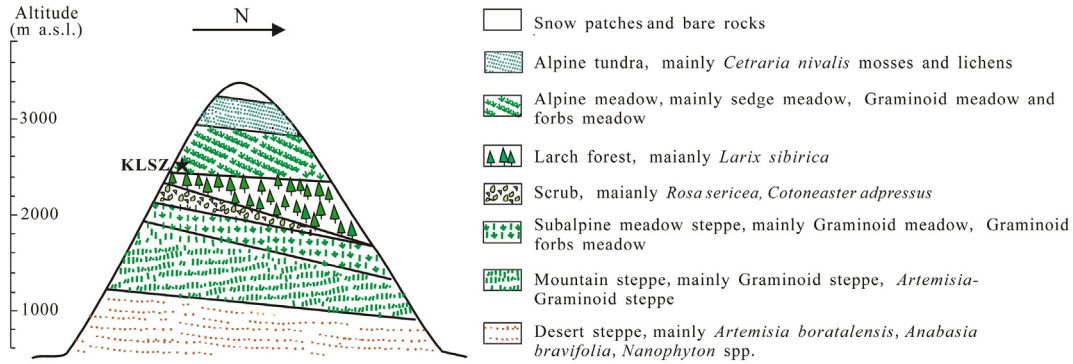
Altitude
(m a.s.l.)
N
3000
2000
1000
KLSZ
Snow patches and bare rocks
Alpine tundra, mainly Cetraria nivalis mosses and lichens
Alpine meadow, mainly sedge meadow, Graminoid meadow and forbs meadow
Larch forest, maianly Larix sibirica
Scrub, maianly Rosa sericea, Cotoneaster adpressus
Subalpine meadow steppe, mainly Graminoid meadow, Graminoid forbs meadow
Mountain steppe, mainly Graminoid steppe, Artemisia-Graminoid steppe
Desert steppe, mainly Artemisia boratalensis, Anabasia bravifolia, Nanophyton spp.

Fig. 2. Vertical vegetation zones in the southern Altai Mountains (Hou, 2001; Yuan, 1986).

Table 1
Dating results of Kelashazi Peat core.

LAB code	Depth (cm)	Dated material	$\delta^{13}C$ (‰)	^{14}C age (yr BP)
AA100613	12	Peat	−25.6	2715 ± 37
AA102016	50	Peat	−25.3	3696 ± 45
AA102062	100	Peat	−26.3	4157 ± 45
AA100617	150	Peat	−26.5	4881 ± 41
AA102063	200	Peat	−24.2	5490 ± 49
AA102064	250	Peat	−25.7	6072 ± 52
AA100616	300	Peat	−26.3	6607 ± 49
AA102065	350	Peat	−26.9	8825 ± 62
AA100615	420	Peat	−27.2	8316 ± 54
AA102066	460	Peat	−25.0	7243 ± 55
AA102067	500	Peat	−26.1	9499 ± 62
AA100614	518	Mud	−25.3	10,200 ± 120
AA102068	530	Mud	−23.5	10,006 ± 64
AA100618	550	Mud	−25.9	10,547 ± 60

spores) were counted for each sample. The percentage of each pollen type was calculated based on the sum of all counted terrestrial pollen grains and the pollen diagrams were plotted using Tilia 1.7.16 software.

3.3. Pollen based indices

3.3.1. Biome score assignment

Biome scores are widely used to reflect major vegetation types (Prentice et al., 1992; Tarasov et al., 1998; Yu et al., 1998) and the scores are based on the contemporary knowledge of the ecology and biogeography of modern plants and associated pollen assemblages (Prentice et al., 1992, 1996). The method consists of four steps: (1) assignment of each pollen taxon to PFTs according to known ecology and biogeography (Table 2); (2) assignment of characteristic PFTs to biomes according to their bioclimatic ranges (Table 3); (3) construction of a biome-by-taxon matrix; and (4) use the formula *(1)* to calculate the affinity scores for all pollen samples.

$$A_{ik} = \sum_j \delta_{ij} \sqrt{\{\max[0, (p_{jk} - \theta_j)]\}} \quad (1)$$

where A_{ik} is the affinity score of pollen sample k for biome i; summation is over all taxa j; δ_{ij} is the entry in the biome taxon matrix for biome i and taxon j; p_{jk} are the pollen percentages, and θ_j is a threshold pollen percentage (0.5% in this study). For each pollen sample, the biome with the highest score is assigned.

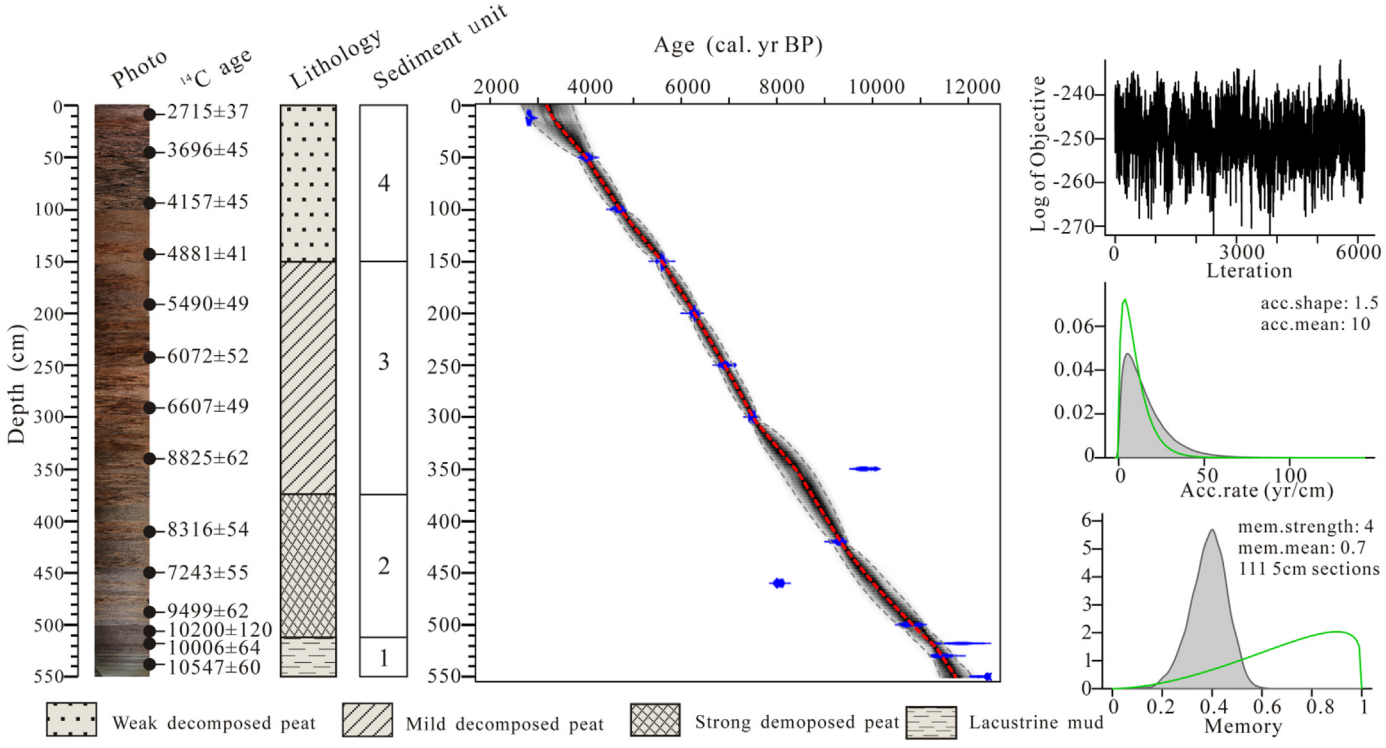

Fig. 3. KLSZ lacustrine-peat core: core photo, dates, strata, and age-depth model.

Table 2
Plant function types (PFTs) and the pollen taxa assigned to them (after Prentice et al., 1996; Tarasov et al., 1998; Yu et al., 2000).

Codes	Trees and shrubs	Pollen taxa
aa	Arctic-alpine dwarf shrub	*Alnus fruticosa-type, Betula nana-type, Gentiana, Pedicularis,* Saxifragaceae
ab	Arctic/boreal dwarf shrub	*Rubus chamaemorus*
bec	Boreal evergreen conifer	*Picea, Pinus* (Haploxylon)
bs	Boreal summer green	*Betula, Larix, Populus, Salix*
bts	Boreal-temperate summer green shrub	*Cornus, Lonicera, Sambucus, Sorbus, Viburnum*
cbc	Cool-boreal conifer shrub	*Pinus* (Haploxylon)
ctc	Cool-temperate conifer	*Abies*
df	Desert forb	Chenopodiaceae, Elaeagnaceae, *Ephedra*, *Nitraria,* Tamaricaeae, Zygophyllaceae
ec	Eurythermic conifer	*Juniperus, Pinus (Diploxylon)*
g	Grass	Poaceae
h	Heath	*Calluna, Cassiope, Empertrum, Ericales, Pyrola, Pyrolaceae*
s	Sedge	Cyperaceae
sf	Steppe forb	*Allium, Anthemis*-type, *Artemisia*, *Aster*-type, Brassicaceae, Campanulaceae, *Cannabis*, Caryophyllaceae, Convolvulaceae, Dipsacaceae, Euphorbiaceae, Fabaceae, *Geraniaceae, Hippophae, Humulus*, *Iridaceae,* Labiatae, *Linaria,* Liliaceae, *Onagraceae,* Papaveraceae, *Plantago,* Plumbaginaceae, *Polygonum, Potentilla, Ranunculaceae, Rosaceae,* Rubiaceae, Rutaceae, *Sanguisorba*, *Saussurea*-type, *Scabiosa, Thalictrum*, *Stellera, Taraxacum*-type, *Utica*
ts	Temperate summer green	*Acer, Euonimus, Fraxinus excelsior-type, Quercus* (deciduous)
ts1	Cool-temperate summer green	*Carpinus, Corylus, Fagus, Frangula, Tilia, Ulmus*
ts2	Warm-temperate summer green	*Castanea, Juglans, Rhamnus, Vitis, Myrica*
wte	Warm-temperate borad-leaved evergreen	*Quercus* (evergreen)

Table 3
Biomes and their characteristic plant functional types (PFTs), PFTs in parentheses are restricted to part of their biome. Abbreviations for PFTs as in Table 2.

Tundra	aa, (ab), g, s, (h)
Cold deciduous forest	bs, ec, cbc, (ab), (h)
Taiga	bs, bec, ab, (bts), ec, (h)
Cold mixed forest	bs, ctc, ec, (bts), (ts1), (h)
Cool conifer forest	bs, bec, ctc, ec, (bts), (ts1), (ab), (h)
Temperate deciduous forest	bs, bts, ctc, ts, ts1, (ts2), wte, ec, h
Cool mixed forest	bs, bec, (ctc), ec, bts, ts, ts1, (h)
Warm mixed forest	ec, (bts), ts, ts1, ts2, wte, h
Steppe	sf, g
Desert	df

Table 4
Simplified vegetation types used in the Vegetation Atlas of China (Hou, 2001) in northern Xinjiang of China and their allocation to the biomes used by Prentice et al. (1992).

Biome name	Vegetation type
Tundra	*Saussurea involocrata*, *Callianthemum alatavicum* sparse vegetation
	Kobresia spp., forb high-cold meadow
	Cetraria nivais tundra
Taiga	*Larix sibirica* forest
	Larix sibirica, *Picea abvata* forest
	Pinus sibirica forest and *Picea sibirica*, *Larix sibirica* forest
Steppe	*Festuca* spp. steppe
	F. spp., forb steppe
	Stipa spp. steppe
	Artemisia frigida steppe
	Seriphidium spp. steppe
	Poa angustifolia steppe
Desert	*Ceratoides latens* desert
	Nanophyton erinaceum desert
	Reaumuria soongorica desert
	Anabasis spp. desert
	Haloxylon persicum and *H. ammodendron* tree – shrub and shrub desert

In this study, some modifications are made according to the studies in former Soviet Union and Mongolia (Tarasov et al., 1998) and also in China (Yu et al., 2000) with a further consideration of the modern vegetation distribution in northern Xinjiang area (Hou, 2001). Specifically, we adopted the method of Yu et al. (1998) and allocated *Artemisia* pollen types to PFT of steppe forb (sf) and Chenopodiaceae to PFT of desert forb (df) (Table 2) because these two have distinct niches in northern Xinjiang area, i.e., the *Artemisia* mainly developed in lower or middle mountain steppe and the Chenopodicaeae extensively developed in desert of dry basins (Table 4). The constructed biome types include tundra, taiga, steppe and desert (Table 4).

3.3.2. Pollen-based quantitative reconstruction of climate

Quantitative climate reconstructions of Kelashazi pollen record are performed using the PFT-MAT (PFT = plant function type; MAT = modern analogue technique) method. The reasons for using PFT-MAT method are fourfold. First, the study area (i.e., southern Altai) is within the PFT-MAT method-used surface pollen data-covered area and the applicability of the surface data can be reasonably assumed. Second, the PFT-MAT method is solely based on numerical matching between modern surface pollen and fossil pollen and does not need to consider the plant physiology and the complicated pollen producing and transporting processes (Guiot et al., 1993; Nakagawa et al., 2002; Overpeck et al., 1985). Third, the PFT-MAT method greatly reduces the 'edge effect' brought by a large calibration set because only five-to-ten analogues with the least numerical distances are used to "read out" the climate variables of the target fossil pollen sample (Birks et al., 2010; Seppä and Bennett, 2003). Fourth, Feng and his colleagues have checked the applicability of the PFT-MAT method in the Altai Mountains area. Specifically, they (Feng et al., 2017) randomly selected 100 pollen data points from the dataset (i.e., totally 2066 data points) falling within a predefined area (i.e., 35–60°N and 70–100°E) that includes the southern Altai and statistically compared the modern pollen-based inferences of the climatic parameters with the corresponding climatic parameters that were either instrument-measured or spatially-interpolated. The correlation coefficient (R) and the root-mean-square error (RMSE) listed in Table 5 indicate that the PFT-MAT is an acceptable method for quantitatively reconstructing the Holocene climate changes in the southern Altai Mountains.

In detail, chord distances between the fossil pollen assemblage and the modern pollen data are calculated for determining the similarity between the fossil and modern pollen spectra (Guiot et al., 1993; Nakagawa et al., 2002; Overpeck et al., 1985). The modern pollen dataset used in the present study includes 1855 surface pollen spectra covering the entire Europe, former Soviet Union territory and Mongolia (Guiot, 1990; Guiot et al., 1993; Tarasov et al., 1998) and 211 surface

Table 5
Statistical comparisons between the modern climate parameters (measured and spatially interpolated) and the climate reconstructions using PFT-MAT (cited from Feng et al., 2017). Pollen data of 100 points were randomly selected from the dataset (i.e., totally 2066 data points) falling within a predefined area (i.e., 35–60°N and 70–100°E) that includes the Kelashazi peat (48°07′N, 88°22′E). Notes: mean January temperature-T_c, mean July temperature-T_w, mean annual temperature-T_{ann}, mean annual precipitation-P_{ann}.

Climatic parameters	Correlation coefficients (R)	R^2	Root mean square error (RMSE)	Significance level (p)
T_c	0.49	0.24	5.83	< 0.001
T_w	0.75	0.56	2.77	< 0.001
T_{ann}	0.65	0.43	3.63	< 0.001
P_{ann}	0.62	0.39	120.25	< 0.001

pollen spectra from northern China (Jiang et al., 2006). To determine the similarity between the fossil and modern pollen spectra, a threshold has to be set to select the 'best modern analogues' (Guiot, 1990; Guiot et al., 1993; Magny et al., 2001, 2003). Specifically, if the chord distance is above a threshold defined by a Monte-Carlo method, the modern samples are considered as poor analogues and not taken into account in the reconstruction. Estimates of climatic parameters are obtained through using a weighted average of the values for five selected best modern analogues, where the weights used are the inverses of the chord distances. All calculations were carried out using the PPPBASE software package (Guiot and Goeury, 1996) and five calculated climatic parameters were: mean January temperature (T_c), mean July temperature (T_w), mean annual temperature (T_{ann}), mean annual precipitation (P_{ann}) and moisture index (i.e., the ratio between the mean annual precipitation (P_{ann}) and the potential evaporation (ET_0)).

4. Results

4.1. Pollen data

The core can be divided into six major pollen assemblage zones (Fig. 4) using the sequential cluster analysis (CONISS).

Pollen Zone A (550–540 cm; ~11,770-~11,630 cal. yr BP) is corresponding to the lower portion of the lacustrine mud layer (Unit 1) and represented by only five samples. The pollen assemblage is absolutely dominated by non-arboreal pollen types. The total pollen concentrations are relatively high with a mean of 38,580 grains per gram. The Cyperaceae and *Artemisia* pollen percentages are moderately high with a mean of 22.87% and 41.87%, respectively. And the *Picea* pollen percentage is relatively low with a mean of 3.21% and the Poaceae pollen percentage is moderately high with a mean of 7.92%.

Pollen Zone B (540–496 cm; ~11,630-~10,800 cal. yr BP) is corresponding to the upper portion of the lacustrine mud layer (Unit 1) and the lowest portion of the strongly decomposed peat layer (Unit 2). The most pronounced features include a dramatic increase of Cyperaceae pollen percentage and a sharp decline of the *Artemisia* pollen percentage. The pollen assemblage is still dominated by non-arboreal pollen types and the total pollen concentration increased slightly. The Cyperaceae pollen percentages increased while the *Artemisia* pollen percentages decreased. Accompanied are the decreases in *Picea* and Poaceae pollen percentages.

Pollen Zone C (496–340 cm; ~10,800-~8230 cal. yr BP) is approximately corresponding to the strongly decomposed peat layer (Unit 2). The pollen assemblage is generally typified by upward increasing trends of *Picea* and Chenopodiaceae pollen percentages and also by a decreasing trend of Poaceae pollen percentage. The *Artemisia* pollen percentage increases at the expense of the Cyperaceae pollen percentage. The total pollen concentration gradually decreases to ~12,000 grains per gram at the end of this pollen zone. Moreover, the drastic changes of major pollen types (including *Artemisia*, Cyperaceae, Poaceae and *Picea*) further divide this zone into three subzones.

Subzone C1 (496–446 cm; ~10,800-~9790 cal. yr BP) is distinguishable by a relatively sharp decrease in Cyperaceae pollen percentage and also by relatively sharp increases in *Artemisia* and Poaceae pollen percentages in comparison with the underlying Pollen Zone B.

Subzone C2 (446–394 cm; ~9790-~9020 cal. yr BP) can be readily discerned by an increase in *Picea* pollen percentage and also by a slight decrease in Poaceae pollen percentage relative to those in the

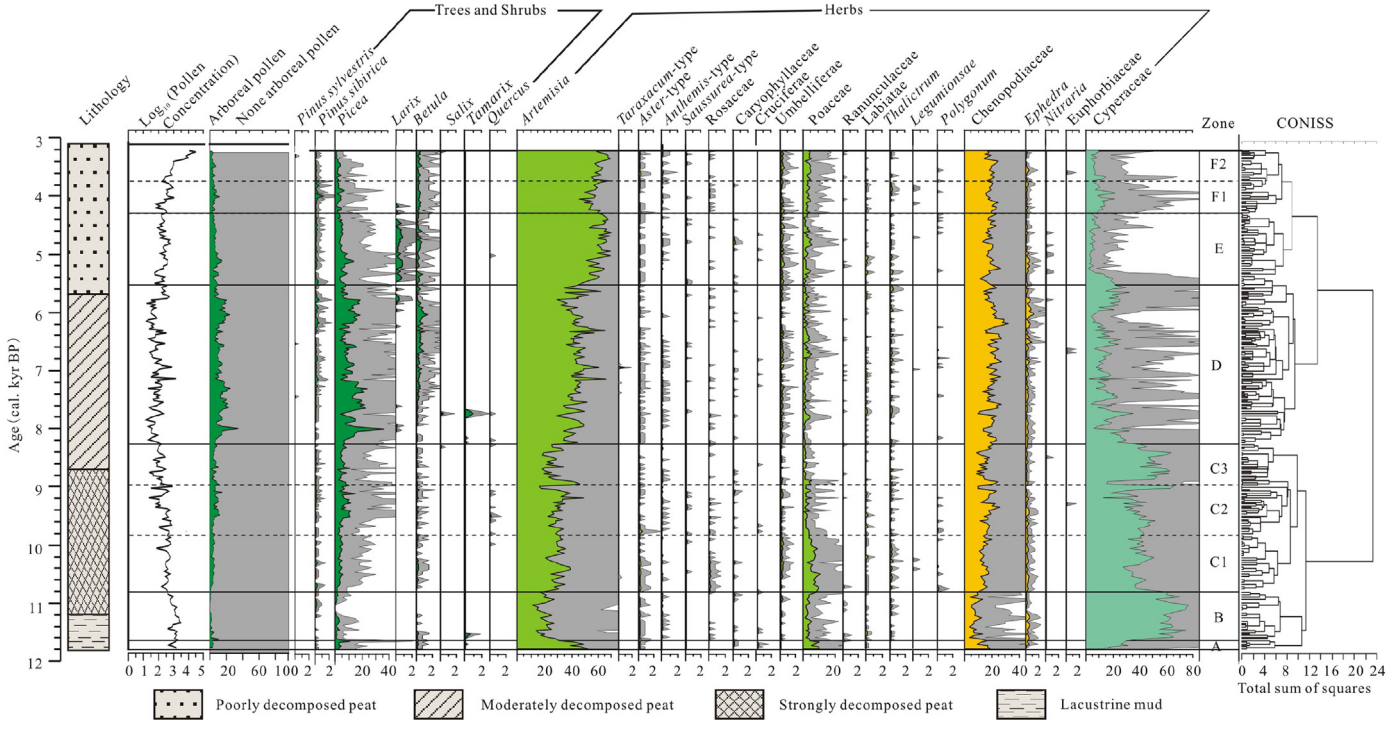

Fig. 4. Chronological and stratigraphic variations of pollen percentages retrieved from KLSZ lacustrine-peat core.

underlying subzone C1. The *Artemisia* and Cyperaceae pollen percentages remain unchanged and the Chenopodiaceae pollen percentage increased slightly.

Subzone C3 (394–340 cm; ~9020-~8230 cal. yr BP) is featured by a jump of Cyperaceae pollen percentage and also by a moderate drop of *Artemisia* pollen percentage at the expenses of *Picea*, Poaceae and Chenopodiaceae pollen percentages.

Pollen Zone D (340–146 cm, ~8230-~5540 cal. yr BP) is approximately corresponding to the moderately decomposed peat layer (Unit 3). The most pronounced features include a peaked pollen percentage of *Picea* and a drastic decrease of Cyperaceae pollen percentage. In addition, deciduous *Betula* pollen percentage increased and *Larix* pollen started to appear at the end of this zone. The *Artemisia* and Chenopodiaceae pollen percentages continued to increase and the total pollen concentration continued to decrease.

Pollen Zone E (146–68 cm; ~5540-~4270 cal. yr BP) is approximately corresponding to the lower part of poorly decomposed peat layer (Unit 4). The distinguishable features are a peak of *Larix* pollen percentage, a peak of *Artemisia* pollen percentage, and a trough of Cyperaceae pollen percentage. In addition, *Picea* pollen percentage decreased dramatically and the total pollen concentration increased slightly.

Pollen Zone F (68–0 cm; ~4270-~3190 cal. yr BP) is corresponding to the upper part of the poorly decomposed peat layer (Unit 4). This pollen assemblage zone is particularly characterized by the disappearance of *Larix* pollen. Cyperaceae pollen percentage increased at the expense of *Artemisia* pollen percentage, and the total pollen concentration increased to a mean of 51,368 grains per gram. The opposite trends between *Artemisia* pollen percentage and Cyperaceae pollen percentage further divide this zone into two subzones (Fig. 4). That is, *Subzone F1* (68–36 cm; ~4270-~3760 cal. yr BP) is readily distinguishable from *Subzone F2* (36–0 cm; ~3760-~3190 cal. yr BP) by an elevated Cyperaceae pollen percentage and also by a lowered *Artemisia* pollen percentage.

4.2. Vegetation dynamics

The pollen assemblages (Fig. 4) and the associated biome scores (Fig. 5) can be used to trace the vegetation successions around the Kelashazi valley. As shown in Fig. 4 and Fig. 5, the vegetation went through six stages of successions.

Vegetation Stage 1 (~11,770-~11,630 cal. yr BP) was the period when the Kelashazi valley was dominated by an alpine meadow (mainly including sedge meadow, Graminoid meadow and forbs meadow), as indicated by high *Artemisia* and Poaceae pollen percentages and a moderate Cyperaceae pollen percentage, and also by the associated higher steppe biome scores (~10) and moderately high tundra biome scores (6–8).

Vegetation Stage 2 (~11,630-~10,790 cal. yr BP) appears to have experienced a deterioration of the previous alpine meadow into a more sedge-dominated alpine tundra, and the deterioration was suggested by an abrupt increase in Cyperaceae pollen percentage at the expenses of *Artemisia*, Chenopodiaceae and Poaceae pollen percentages. The inferred deterioration was also suggested by a decrease in steppe biome scores (~7) and an increase in tundra biome scores (~10).

Vegetation Stage 3 (~10,790-~8230 cal. yr BP) was the time interval when the deteriorated vegetation (i.e., alpine tundra) returned to an alpine meadow, being similar to that of Vegetation Stage 1.

Vegetation Stage 4 (~8230-~5540 cal. yr BP) was characterized by an admixture of dark taiga forest components (spruce) and alpine meadow components (sedge and Graminoid), suggesting a rise of the alpine tree line. This inference was based on the following observations: a peaked *Picea* pollen percentage, increased *Artemisia* and Chenopodiaceae pollen percentages, the highest taiga biome score (~4) of the entire core, a moderately high steppe biome score (~10), and a relatively low tundra biome score (~4).

Vegetation Stage 5 (~5540-~4270 cal. yr BP) was typified by the following characteristics: a peaked *Larix* pollen percentage, decreased *Picea* and Cyperaceae pollen percentages, and an increased *Artemisia* pollen percentage. Overall, the taiga biome score (2–4) decreased and the steppe biome score (11 − 12) increased. Considering the fact that *Larix* pollen is generally under-represented in pollen records due to its low productivity and weak dispersal capacity (Niemeyer et al., 2015; Sjögren et al., 2008) so that a rather low *Larix* pollen percentage is usually accepted as evidence for local presence of *Larix* forests (Edwards et al., 2005), we speculate that the former *Picea*-dominated dark taiga forests (i.e., Vegetation Stage 4) might have been replaced by *Larix*-dominated light taiga forests, accompanied with an expansion of the alpine meadows.

Vegetation Stage 6 (~4270-~3190 cal. yr BP) witnessed a dramatic reduction in arboreal pollen percentages with a complete disappearance of *Larix* pollen. The relatively high *Artemisia* and Chenopodiaceae pollen percentages, together with rather high steppe biome scores (~12), rather low taiga biome scores (~2) and increased tundra biome scores (~4), suggest that the alpine upper tree line descended and the alpine meadow expanded.

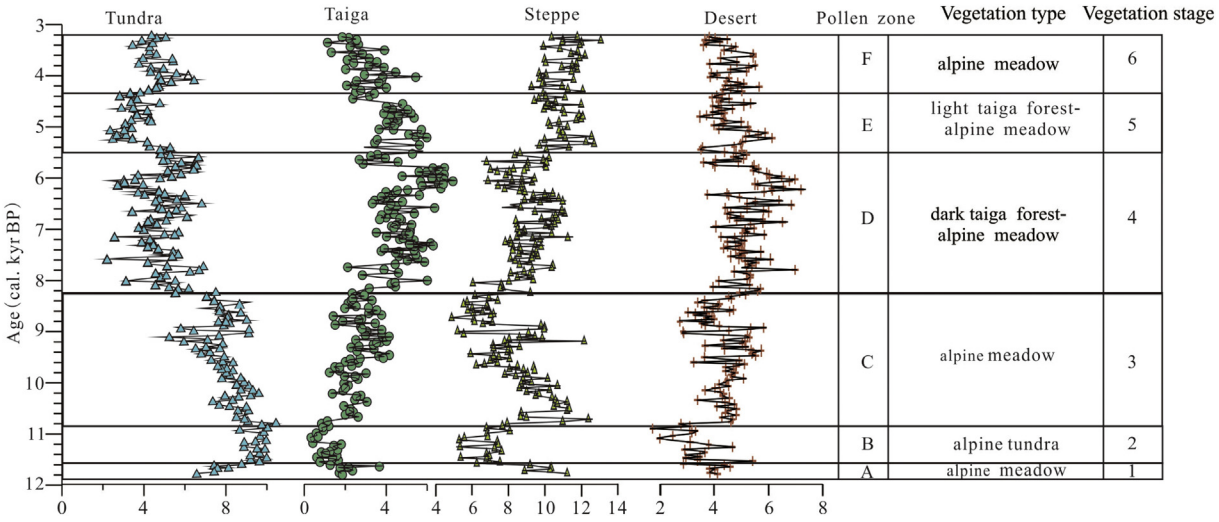

Fig. 5. Biome scores of the KLSZ lacustrine-peat core and the associated vegetation types.

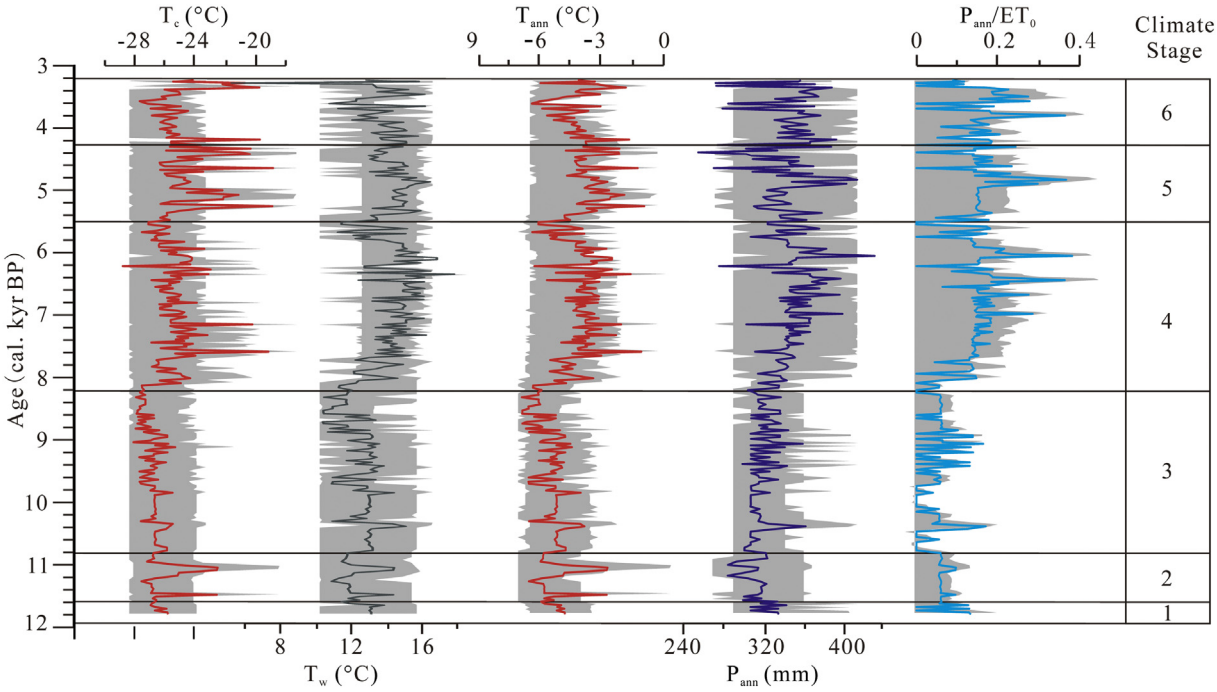

Fig. 6. Pollen-based estimates of temperatures (T_c, T_w and MAT), precipitation (P_{ann}) and P_{ann}/ET_0 from KLSZ pollen data.

4.3. Climate change

The inference of the climate change in the Kelashazi valley is based on the PFT-MAT estimates of five parameters (i.e., T_c, T_w, T_{ann}, P_{ann} and P_{ann}/ET_0) with references to the pollen assemblages (Fig. 6).

Climate Stage 1 (~11,770-~11,630 cal. yr BP) experienced a cold and dry climate.

Climate Stage 2 (~11,630-~10,800 cal. yr BP) witnessed an averagely cold and dry climate, as indicated by those quantitative estimates.

Climate Stage 3 (~10,800-~8230 cal. yr BP) was slightly warmer (e.g., T_w, T_{ann}) than the preceding stage (i.e., Climate Stage 2) and significantly cooler than the succeeding stage (i.e., Climate Stage 4). The estimated P_{ann} of Climate Stage 3 was slightly higher than that in the preceding stage and significantly lower than that in the succeeding stage. However, it is rather noticeable that the estimated moisture index (i.e., P_{ann}/ET_0) was the lowest of the entire core. It is also noticeable that the PFT-MAT estimate of the January temperature (T_c) was also the lowest of the entire core.

Climate Stage 4 (~8230-~5540 cal. yr BP) was characterized by the highest July temperature (T_w) with the January temperature (T_c) being lower than that in the succeeding stage (i.e., Climate Stage 5). The estimated mean annual precipitation (P_{ann}) and moisture index (P_{ann}/ET_0) were on average significantly higher than those in the preceding stage (i.e., Climate Stage 3) and slightly lower than those in the succeeding stage (i.e., Climate Stage 5).

Climate Stage 5 (~5540-~4270 cal. yr BP) was characterized by the following features in comparison with the preceding stage (i.e., Climate Stage 4): (a) an averagely higher T_c with a higher amplitude of fluctuations, (b) a slightly lowered T_w, (c) a slightly lowered P_{ann}. Overall, the reconstructed mean annual temperature (T_{ann}) and P_{ann}/ET_0 are similar to those in the preceding stage (i.e., Climate Stage 4). Two facts standing out in Fig. 4 appear to suggest that the mean annual temperature (T_{ann}) in Climate Stage 5 was either averagely cooler (Prokopenko et al., 2007) or the January temperature (T_c) fluctuated with a rather high amplitude (Shi et al., 2008) relative to those in the preceding stage (i.e., Climate Stage 4). The first fact is that the *Larix* pollen percentage reached the highest of the entire core, probably suggesting an averagely cooler climate. And, the second fact is that the *Picea* pollen percentage dropped dramatically, seemingly implying a high-amplitude fluctuation in January temperature. However, due to the acknowledged lower representation of *Larix* pollen signature (Shi et al., 2008), the significant appearance of *Larix* pollen grains in Climate Stage 5 implies that the quantitatively-reconstructed temperatures were likely overestimated.

Climate Stage 6 (~4270-~3190 cal. yr BP) appears to have witnessed a cool and wet climate as indicated by decreases in all three temperature parameters (T_c, T_w and T_{ann}). The estimated P_{ann} and the calculated P_{ann}/ET_0 ratio remained at relatively high levels.

5. Discussion

5.1. Holocene thermal maximum in the AAZ core area

As shown in Fig. 7, the mean annual temperature reconstructed from Kelashazi lacustrine-peat core remained low prior to ~8.0 cal. kyr BP and experienced a mid-Holocene thermal maximum lasting from ~8.0 to ~5.6 cal. kyr BP (Fig. 7a). The corresponding taiga biome score was the highest of the entire core (Fig. 7b), suggesting an expansion of taiga forests during the maximum. This mid-Holocene thermal maximum is reasonably corroborated by several recently-published and relatively well-dated sequences from nearby sites (see Fig. 1a for site locations). For example, the peak of *Picea* pollen percentage spanning from ~8.0 to ~6.5 cal. kyr BP in Kanas Lake core (Fig. 7c) suggests an expansion of taiga forests under a warmer condition in the watershed (Huang et al., 2018). The PCA axis 1 of pollen types in Tielishahan Peat core near Kanas Lake (Fig. 7d) was interpreted to indicate a warm climate from ~7.8 to ~5.4 cal. kyr BP (Zhang et al., 2018b). In addition, the GDGTs data (Fig. 7e) in Habahe Peat core also near Kanas Lake demonstrated a high warm-season temperature interval spanning from ~8.0 to ~5.6 cal. kyr (Tang, 2014). Towards north from Kanas Lake is the Belukha Glacier and the $\delta^{18}O$ record from the ice core (Fig. 7f) exhibits a prolonged warm period lasting from ~8.8 to ~4.0 cal. kyr BP (Aizen et al., 2016).

Towards southeast from Kanas Lake is Balikun Lake and the C_{37} data retrieved from the lake core (Fig. 7g) was interpreted to display a high warm-season temperature from ~8.4 to ~5.6 cal. kyr BP (Zhao et al.,

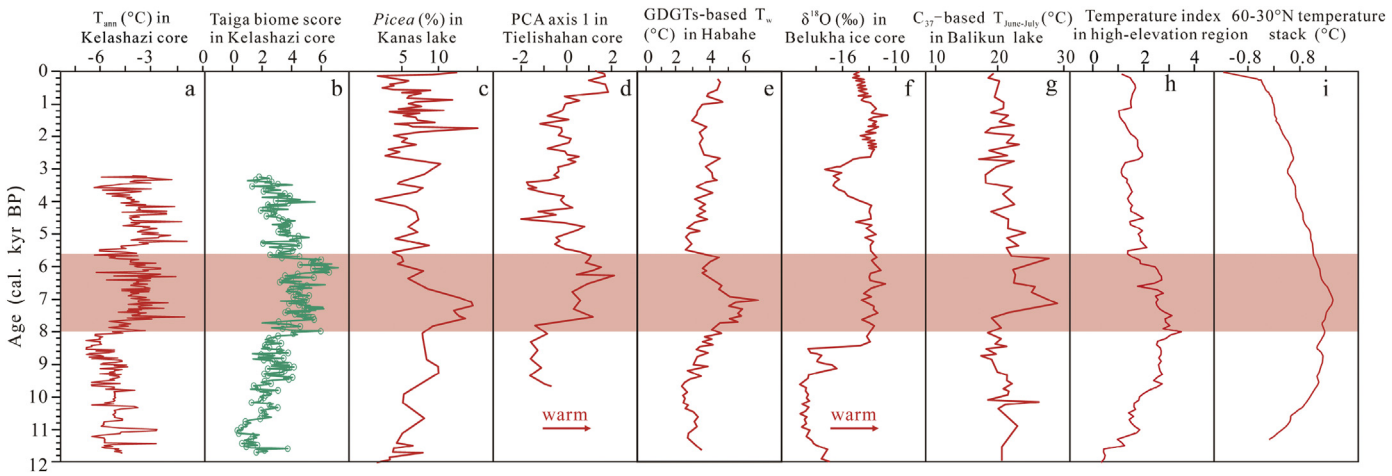
T_{ann} (°C) in Kelashazi core
Taiga biome score in Kelashazi core
Picea (%) in Kanas lake
PCA axis 1 in Tielishahan core
GDGTs-based T_w (°C) in Habahe
$\delta^{18}O$ (‰) in Belukha ice core
C_{37}-based $T_{June-July}$ (°C) in Balikun lake
Temperature index in high-elevation region
60-30°N temperature stack (°C)
Age (cal. kyr BP)
warm
warm

Fig. 7. Comparisons of records from Kelashazi Peat (T_{ann} sequence (a) and taiga biome score sequence (b)) with the temperature records from nearby sites. Included are: *Picea* pollen percentage in Kanas Lake core (c) (Huang et al., 2018), PCA axis 1 of pollen data in Tielishahan Peat core (d) (Zhang Y. et al., 2018), GDGTs-based warm season temperature in Habahe Peat core (e) (Tang, 2014), $\delta^{18}O$ record in Belukha ice core (f) (Aizen et al., 2016), C_{37}-based summer temperature in Balikun Lake core (g) (Zhao et al., 2017), pollen-based temperature index in high-elevation regions of the Altai Mountains and the surrounding areas (h) (Zhang and Feng, 2018), and 60–30°N temperature stack (i) (Marcott et al., 2013).

2017). Again, this mid-Holocene thermal maximum is reasonably corroborated by the data from the aforementioned sequences. Far more important is the fact that this mid-Holocene thermal maximum is in a good agreement with the pollen-based temperature index-indicated thermal maximum in high-elevation regions in the Altai Mountains and the surrounding areas (Fig. 7h; Zhang and Feng, 2018). The pollen-based temperature index-indicated thermal maximum in high-elevation regions was also consistent with the maximum of temperature stack for 60–30°N (Fig. 7i; Marcott et al., 2013). The onset of the warming at Kelashazi Peat is more sudden and later than in 60–30°N temperature stack. However, this later onset can be explained by the cooling influence of remnant ice sheets in the early Holocene (Renssen et al., 2009, 2012).

5.2. Holocene moisture trend in the AAZ core area

As shown in Fig. 8a, Kelashazi moisture (i.e., P_{ann}/ET_0) was persistently low before ~8.0 cal. kyr BP and persistently high with a high-amplitude fluctuation afterward (i.e., from ~8.0 to ~3.2 cal. kyr BP). The persistent dry conditions before ~8.0 cal. kyr BP and persistent wet conditions after ~8.0 cal. kyr BP were relatively well corroborated by several recently- published moisture sequences from the southern Altai and also from the adjacent Junggar Basin (see Fig. 1a for site locations). For example, the (*Juniperus* + *Ephedra*)-indicated moisture sequence from Kanas Lake lends a rather strong support to Kelashazi moisture sequence (Fig. 8b; Huang et al., 2018). Furthermore, the pollen-based RDI (Reconnaissance Drought Index) sequence from Narenxia Peat near Kanas Lake (Fig. 8c; Zhang et al., 2018a) and the humification-indicated moisture sequence from Tielishahan Peat also near Kanas Lake (Fig. 8d; Zhang et al., 2016) are supportive to Kelashazi moisture sequence. In addition, four moisture sequences from the Junggar Basin also lend supports to Kelashazi moisture sequence. Specifically, the A/E ratio sequence from Wulungu Lake in the northern margin of the Junggar Basin (Fig. 8e; Liu et al., 2008) and the peat

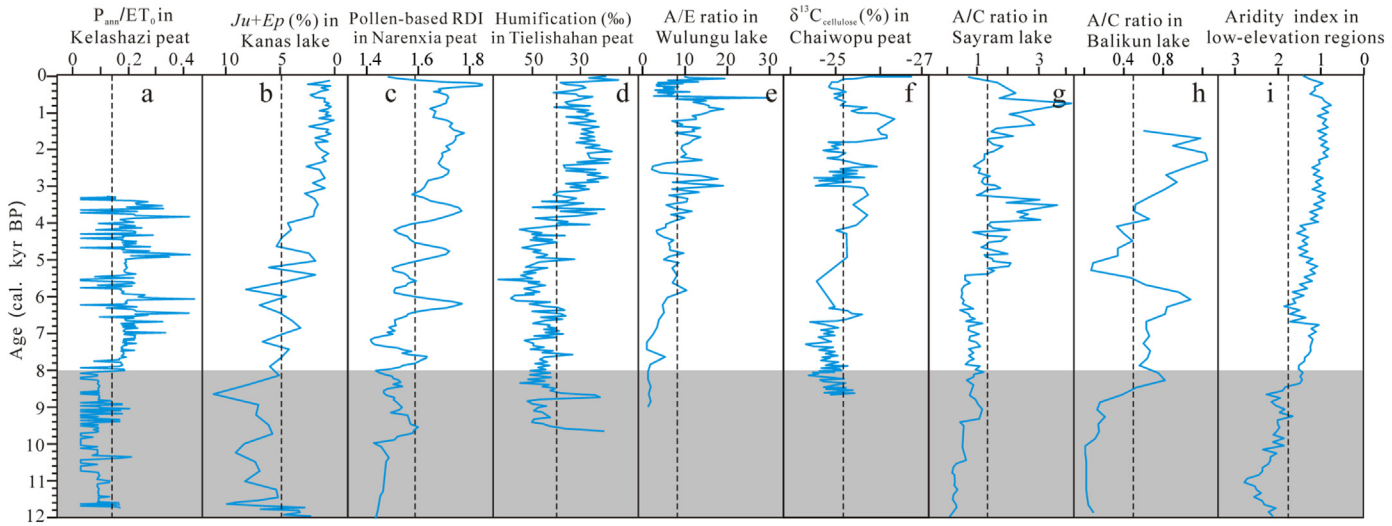
P_{ann}/ET_0 in Kelashazi peat
Ju+Ep (%) in Kanas lake
Pollen-based RDI in Narenxia peat
Humification (‰) in Tielishahan peat
A/E ratio in Wulungu lake
$\delta^{13}C_{cellulose}$ (‰) in Chaiwopu peat
A/C ratio in Sayram lake
A/C ratio in Balikun lake
Aridity index in low-elevation regions
Age (cal. kyr BP)

Fig. 8. Comparisons of Holocene moisture from Kelashazi Peat (a: pollen-based P_{ann}/ET_0) with the moisture records from nearby sites. b: (*Juniperus* + *Ephedra*)% sequence from Kanas Lake (Huang et al., 2018); c: Pollen-based RDI (Reconnaissance Drought Index) sequence from Narenxia Peat (Zhang et al., 2018a); d: humification-indicated moisture sequence from Tielishahan Peat (Zhang et al., 2016); e: A/E ratio sequence from Wulungu Lake (Liu et al., 2008); (f) $\delta^{13}C_{celluose}$ sequence from Chaiwopu Peat (Hong et al., 2014); (g) A/C ratio sequence from Sayram Lake (Jiang et al., 2013); (h) A/C ratio sequence from Balikun Lake (An et al., 2012); (i) synthesized aridity index sequence in low-elevation regions of the Altai Mountains and the surrounding areas (Zhang and Feng, 2018).

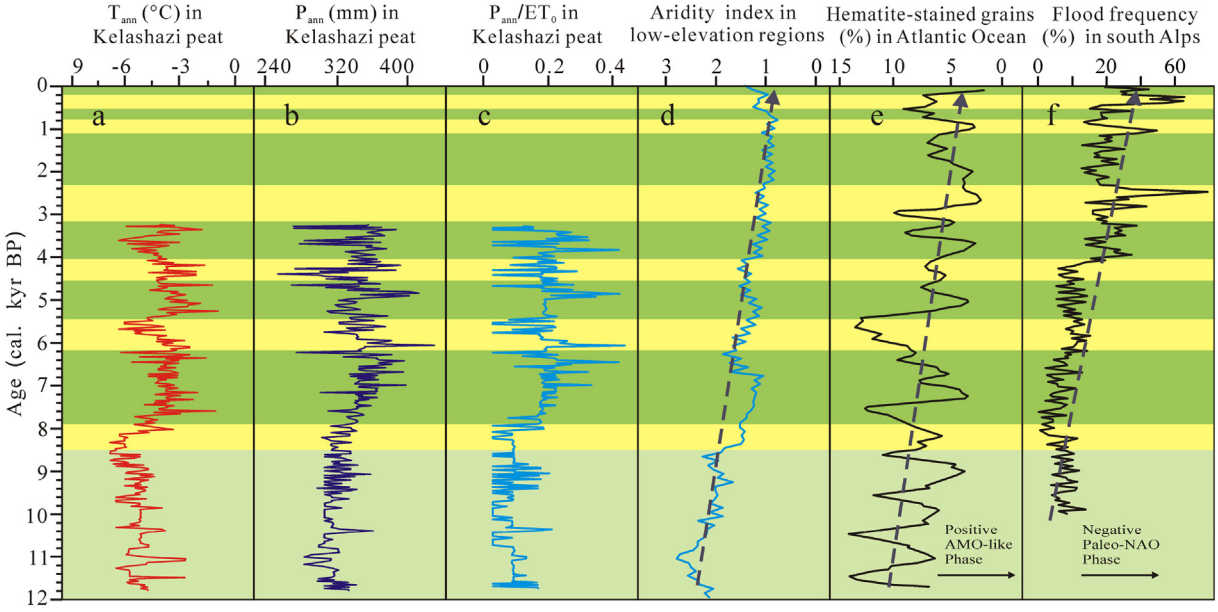

Fig. 9. Possible driving mechanisms of Holocene moisture sequences in AAZ core area. a: pollen-based T_{ann} sequence at Kelashazi Peat (this study); b: pollen-based P_{ann} sequence at Kelashazi Peat (this study); c: pollen-based P_{ann}/ET_0 sequence at Kelashazi Peat (this study); d: synthesized aridity index sequence in low-elevation regions of the Altai Mountains and the surrounding areas (Zhang and Feng, 2018); e: hematite-stained grains (%) in the North Atlantic Ocean (Bond et al., 1997) as a proxy for AMO-like events (i.e., Atlantic Multi-centennial Oscillations) in North Atlantic (Feng et al., 2009); f: NAO (i.e., North Atlantic Oscillations) variations as suggested by the flood frequency data in south Alps (Wirth et al., 2013).

$\delta^{13}C_{celluose}$ sequence from Chaiwopu Peat in the southern margin of the Junggar Basin (Fig. 8f; Hong et al., 2014) are in a broad agreement with Kelashazi moisture sequence. And, the A/C ratio sequence from Sayram Lake in the western margin of the Junggar Basin (Fig. 8g; Jiang et al., 2013) and the A/C ratio sequence from Balikun Lake (Fig. 8h; An et al., 2012) are also in a broad agreement with Kelashazi moisture sequence. Far more important is the fact that the synthesized aridity index curve, based on 19 pollen sequences, for low-elevation regions in the Altai Mountains and the surrounding areas (Fig. 8i; Zhang and Feng, 2018) is in unexpectedly high agreement with Kelashazi moisture curve although the top portion (i.e., the past ~3200 years) was missing in the Kelashazi sequence.

5.3. Possible driving mechanisms

5.3.1. AMO-like events and trend

The pollen-based reconstructions (T_{ann}, P_{ann} and P_{ann}/ET_0) from Kelashazi peat (Fig. 9a-c) display two-order climate changes during the data-covering period (i.e., from ~12.0 to ~3.2 cal. yr BP). The first-order changes refer to the two major stages of climate change: a rather cold and dry early Holocene spanning from ~12 to ~8.0 cal. kyr BP and a relatively warm and wet middle Holocene lasting from ~8.0 to ~3.2 cal. kyr BP. The second-order variations refer to the lows and highs superimposed on the first-order change. In addition, the moisture curve, a synthesis of 11 pollen sequences, for the low-elevation regions within the Altai Mountains and the surrounding areas appears to be more or less corroborative with the pollen-based P_{ann}/ET_0 curve (Fig. 9d; Zhang and Feng, 2018) not only in the first-order changes but also in the second-order variations if the uncertainties in the chronologies are fully considered. Furthermore, the increasing precipitation and rising moisture reconstructions (P_{ann} and P_{ann}/ET_0) from Kelashazi Peat and also the wetting curve for the low-elevation regions are approximately correspondent with the reducing percentages of the hematite-stained grains in the North Atlantic (Fig. 9e) again not only in the first-order changes but also in the second-order variations if the uncertainties in the chronologies are fully considered. The hematite-stained grain-recorded IRD events (Bond et al., 1997) were demonstrated to be AMO-like events (Feng et al., 2009), i.e., low hematite-stained grains corresponded to positive AMO-like events. The millennial-scale AMO-like events in the North Atlantic Ocean might have not only controlled the climate in northern Europe (Bakkle et al., 2008) but also the climate in the study area (Sun et al., 2015). It means that positive AMO-like events may have brought more winter precipitation supplies to the study area via northern Europe. It also means that positive AMO-like events might have also brought more summer precipitation to the study area via its interactions with the North Pacific Ocean. The interactions between AMO and the North Pacific Ocean are revealed by modern observations (Sun et al., 2015). That is, an east-west dipole structure covering the core of the Eurasian continent leads to an intensification of the transport of vertically integrated water vapor flux mainly from the North Pacific Ocean during the positive AMO phases, favoring the increase of precipitable water flux in the study area. Again, as proposed by Zhang and Feng (2018), the Holocene wetting trend and the wetter intervals along the trend in the Altai Mountains and the surrounding areas might have been modulated by the AMO-like trend and fluctuations in the North Atlantic.

5.3.2. NAO trend

North Atlantic Oscillations (NAO) have been proposed to be the dominant forcing factor not only in shaping the modern climate of the AAZ core area (Aizen et al., 2001; Bridgman and Oliver, 2006; Meeker and Mayewski, 2002; Hurrell, 1996), but also in shaping the Holocene climate of the AAZ core area (Chen et al., 2008; Feng et al., 2017; Ran and Feng, 2013). A recent reconstruction of the Holocene NAO variations does lend a strong support to the propositions. Wirth et al. (2013) demonstrated that more floods occurred in the south Alps under negatively-phased NAO settings during the Holocene. The flood frequency-indicated Paleo-NAO curve (Fig. 9f; Wirth et al., 2013) exhibits more or less a parallel more negative trend with the pollen-based P_{ann}/ET_0 curve from Kelashazi Peat during the data-overlapping period (i.e., from ~12.0 to ~3.2 cal. kyr BP) and also with the moisture curve for the low-elevation regions within the Altai Mountains and the surrounding areas during the data-overlapping period (i.e., the past ~10,000 years). It means that the Holocene warming trend in the sea

surface of the North Atlantic might have causally led to more and more negatively-phased NAO activities through gradually reducing the pressure gradient between the Azores High and the Icelandic Low. The Holocene increasing trend of negatively-phased NAO activities means more and more Atlantic storm tracks in the southern part of the North Atlantic and also in the Mediterranean Sea (Wirth et al., 2013). The negatively-phased NAO-resulted storm tracks have been instrumentally documented to be rather powerful during winters in transporting precipitable water vapor to the Altai Mountains and the surrounding areas primarily along the northern piedmonts of the Tianshan Mountains (Kutzbach et al., 2014; Huang et al., 2015). The positively-phased AMO activities were demonstrated to be rather effective during summers in bringing more precipitable water vapor to the southern Siberia and the adjacent Altai Mountains via their interactions with the North Pacific Decadal Oscillations (PDO) (Sun et al., 2015). That is, the Holocene increasing trend (Fig. 9d) of the moisture in low-elevation regions within the Altai Mountains and the surrounding areas might have resulted not only from the increasing trend of NAO-related winter precipitation but also from the increasing trend of AMO-related summer precipitation.

5.3.3. A dilemma

We are now facing a dilemma to reconcile the site-based reconstructions of the average annual temperature (T_{ann}) and the moisture index (P_{ann}/ET_0) from Kelashazi peat with the regional syntheses of temperature and aridity index from both low-elevation regions and high-elevation regions. As mentioned earlier in section 5.1. (Holocene thermal maximum in the AAZ core area), the mid-Holocene thermal maximum lasting from ~8.0 to ~5.6 cal. kyr BP (Fig. 10a) from Kelashazi Peat, a high-elevation site (2422 m a.s.l.), is in a good agreement with the 11 pollen sequences-based temperature index-indicated thermal maximum in high-elevation regions in the Altai Mountains and the surrounding areas (Fig. 10c; Zhang and Feng, 2018), being much later than that in low-elevation regions (Fig. 10b). The dilemma we are facing is the fact that the pollen-based moisture curve from Kelashazi Peat is not in a good agreement with the pollen-based aridity curve from high-elevation regions (Fig. 10f). Instead, the moisture curve from Kelasazi Peat is in a good agreement with the 19 pollen sequences-based aridity curve from low-elevation regions (Fig. 10e; Zhang and Feng, 2018). The thermal maximum lasting from ~8.0 to ~5.6 cal. kyr BP in high-elevation regions was interpreted to be consistent with 60–30°N thermal maximum spanning from ~8.0 to ~6.0 cal. kyr BP (Marcott et al., 2013). The sudden and later onset of warming in high-elevation regions was speculated to be associated with the remnant ice sheets in the early Holocene (Renssen et al., 2009, 2012). That is, the remnant ice sheets not only lowered the temperature but also raised the moisture levels in high-elevation regions during the early Holocene. The question is: why was the early Holocene moisture level in Kelashazi Peat, a high-elevation site (2422 m a.s.l.), not raised (Fig. 10d)? The reason for the unexpected low moisture levels in the early Holocene might be related with the southeastern (i.e., dry) location of Kelashazi Peat (48°07′N, 88°22′E). That is, the southeastern site was likely directly influenced by the air masses that were massively cooled by remnant ice sheets over the Siberia and the adjacent northern Altai Mountains in the early Holocene, while the remnant ice sheets in this southeastern (i.e., dry) location was not thick enough to sustain a high moisture level in the early-Holocene.

6. Conclusions

1) The pollen assemblages and the associated biome scores suggest that the vegetation in Kelashazi valley was dominated by alpine meadows during the early Holocene before ~8.2 cal. kyr BP and by taiga forests in the middle Holocene (from ~8.2 to ~5.6 cal. kyr BP) that was followed by an expansion of alpine meadows (from ~5.6 to ~3.2 cal. kyr BP).
2) The pollen-based temperature index-indicated thermal maximum lasting from ~8.0 to ~5.6 cal. kyr BP in high-elevation regions including Kelashazi Peat was interpreted to be more sudden and later than in 60–30°N temperature stack and this later onset can be explained by the cooling influence of remnant ice sheets in the early Holocene.
3) The pollen-based increasing moisture index curve from Kelashazi Peat is in a good agreement with the synthesized aridity index curve for low-elevation regions in the Altai Mountains and the surrounding areas during the data-overlapping period (from ~12.0 to ~3.2 cal. kyr BP).
4) The Holocene increasing trend of moisture at Kelashazi Peat and also in low-elevation regions within the Altai Mountains and the surrounding areas might have resulted not only from the increasing

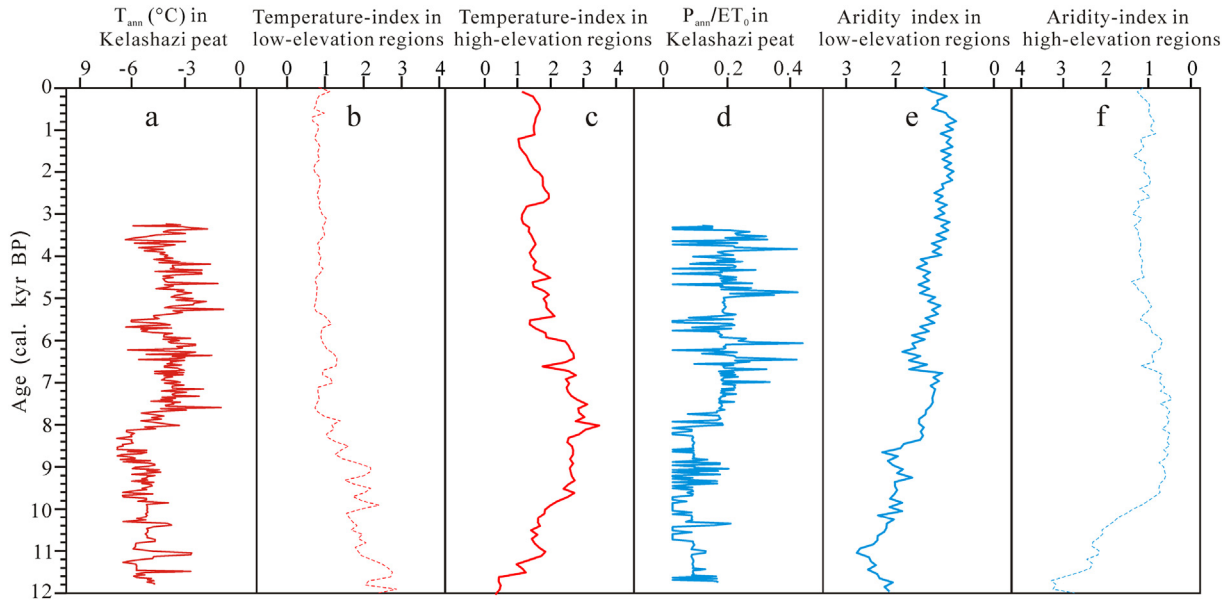

Fig. 10. Comparisons of T_{ann} sequence (a) and P_{ann}/ET_0 sequence (d) from Kelashazi Peat (this study) with synthesized temperature index (b) and aridity index (e) in low-elevation regions and also with synthesized temperature index (c) and aridity index (f) in high-elevation regions (Zhang and Feng, 2018).

trend of NAO-related winter precipitation but also from the increasing trend of AMO-related summer precipitation.

Acknowledgement

This research was financially supported by Chinese Natural Science Grants (No. 41771234 and No. 41562009) and Postdoctoral Innovative Talent Support Program of China (No. BX20190363). We thank Prof. ABDUSALIH Nurbayev, Dr. SUN Aizhi, Dr. RAN Min, Dr. LAN Bo and Dr. YANG Yunpeng for their assistance.

References

Abdusalih, N., Thevs, N., Abzar, A., Chen, K.L., Joosten, H., 2008. Peat-lands of the Chinese Altay. Peat Lands Int. 2, 25–29.
Aizen, E.M., Aizen, V.B., Melack, J., Nakamura, T., Ohta, T., 2001. Precipitation and atmospheric circulation patterns at mid-latitudes of Asia. Int. J. Climatol. 21 (5), 535–556.
Aizen, E.M., Aizen, V.B., Takeuchi, N., Mayewski, P.A., Grigholm, B., Joswiak, D.R., Nikitin, S.A., Fujita, K., Nakawo, M., Zapf, A., Schwikowski, M., 2016. Abrupt and moderate climate changes in the mid-latitudes of Asia during the Holocene. J. Glaciol. 62 (233), 411–439.
An, C.B., Lu, Y., Zhao, J., Tao, S., Dong, W., Li, H., Jin, M., Wang, Z., 2012. A high resolution record of Holocene environmental and climatic changes from Lake Balikun (Xinjiang, China): implications for central Asia. Holocene 22, 43–52.
Bakkle, J., Lie, O., Dahl, S., Nesje, A., Bjune, A.E., 2008. Strength and spatial patterns ofthe Holocene wintertime westerlies in the NE Atlantic region. Glob. Planet. Chang. 60, 28–41.
Birks, H.J.B., Oliver, H., Seppä, H., Bjune, A.E., 2010. Strengths and weaknesses of quantitative climate reconstructions based on late-quaternary biological proxies. Open Ecol. J. 3, 68–110.
Blaauw, M., 2010. Methods and code for 'classical' age-modelling of radiocarbon sequences. Quat. Geochro. 5 (5), 512–518.
Bond, G., Shower, W., Cheseby, M., Lotti, R., Almasi, P., deMenocal, P., Priore, P., Cullen, H., Hajdas, I., Bonani, G., 1997. A pervasive millennial-scale cycle in North Atlantic Holocene and Glacial climates. Science 278, 1257–1266.
Bridgman, B.H., Oliver, J.E., 2006. The Global Climate System, Patterns, Processes, and Teleconnections. Cambridge University Press, New York, pp. 25–54.
Chen, X., 2010. Geography of Chinese Arid Region. Science Press, Beijing.
Chen, F.H., Yu, Z., Yang, M., Ito, E., Wang, S., Madsen, D., Huang, X., Zhao, Y., Sato, T., Birks, H., Boomer, I., Chen, J., An, C., Wunnemann, B., 2008. Holocene moisture evolution in arid Central Asia and its out-of-phase relationship with Asian monsoon history. Quat. Sci. Rev. 27, 351–364.
Chen, F.H., Jia, J., Chen, J., Li, G., Zhang, X., Xie, H., Xia, D., Huang, W., An, C., 2016. A persistent Holocene wetting trend in arid central Asia, with wettest conditions in the late Holocene, revealed by multi-proxy analyses of loess-paleosol sequences in Xinjiang, China. Quat. Sci. Rev. 146, 134–146.
Cheng, H., Zhang, P., Spotl, C., Edwards, R., Cai, Y., Zhang, D., Sang, W., Tan, M., An, Z., 2012. The climatic cyclicity in semiarid-arid central Asia over the past 500,000 years. Geophys. Res. Lett. 39, L01705.
Cheng, H., Spoetl, C., Breitenbach, S., Sinha, A., Wassenburg, J., Jochum, K., Scholz, D., Li, X., Yi, L., Peng, Y., Lv, Y., Zhang, P., Votintseva, A., Loginov, V., Ning, Y., Kathayat, G., Edwards, R., 2016. Climate variations of Central Asia on orbital to millennial timescales. Sci. Re. 6, 36975.
Edwards, M.E., Brubaker, L.B., Lozhkin, A.V., Anderson, P.M., 2005. Structurally novel biomes: a response to past warming in Beringia. Ecology 86, 1696–1703.
Feng, S., Hu, Q., Oglesby, R.J., 2009. AMO-like variations of Holocene sea surface temperatures in the North Atlantic Ocean. Clim. Past. Discu. 5, 2465–2496.
Feng, Z., Sun, A., Abdusalih, N., Ran, M., Kurban, A., Lan, B., Zhang, D., Yang, Y., 2017. Vegetation changes and associated climatic changes in the southern Altai Mountains within China during the Holocene. Holocene 27, 683–693.
Gong, D.Y., Ho, C.H., 2002. The Siberian High and climate change over middle to high latitude Asia. Theor. Appl. Climatol. 72, 1–9.
Gong, D., Wang, S., Zhu, J., 2001. East Asian winter monsoon and Arctic oscillation. Geogr. Res. Lett. 28, 2073–2076.
Guiot, J., 1990. Methodology of the last climatic cycle reconstruction in France from pollen data. Palaeogeogr. Palaeoclimatol. Palaeoecol. 80 (1), 49–69.
Guiot, J., Goeury, C., 1996. PPPBASE, a software for statistical analysis of paleoecological and paleoclimatological data. Dendrochronologia 14, 295–300.
Guiot, J., Debeaulieu, J., Cheddadi, R., David, F., Ponel, P., Reille, M., 1993. The climate in western-Europe during the last glacial interglacial cycle derived from pollen and insect remains. Palaeogeogr. Palaeoclimatol. Palaeoecol. 103, 73–93.
Harrison, S.P., Yu, G., Tarasov, P.E., 1996. Late Quaternary lake-level record from Northern Eurasia. Quat. Res. 45, 138–l 59.
Herzschuh, U., 2006. Palaeo-moisture evolution in monsoonal Central Asia during the last 50,000 years. Quat. Sci. Rev. 25 (1–2), 163–178.
Hilbig, W., 1995. The Vegetation of Mongolia. SPB Academic Publishing, Amsterdam, pp. 89–119.
Hong, B., Gasse, F., Uchida, M., Hong, Y., Leng, X., Shibata, Y., An, N., Zhu, Y., Wang, Y., 2014. Increasing summer rainfall in arid eastern-Central Asia over the past 8500 years. Sci. Rep. 4, 5279.
Hou, X., 2001. Vegetation Atlas of China. Science Press, Beijing, pp. 260.
Huang, W., Chen, J.H., Zhang, X.J., Feng, S., Chen, F.H., 2015. Definition of the core zone of the "westerlies-dominated climatic regime", and its controlling factors during the instrumental period. Sci. China Earth Sci. 58, 676–684.
Huang, X.Z., Peng, W., Rudaya, N., Grimm, E.C., Chen, X.M., Cao, X.Y., Zhang, J., Pan, X.D., Liu, S.S., Chen, C.Z., Chen, F.H., 2018. Holocene vegetation and climate dynamics in the Altai Mountains and surrounding areas. Geophys. Res. Lett. 45 (13), 6628–6636.
Hurrell, J.W., 1996. Influence of variations in extratropical wintertime teleconnections on Northern Hemisphere temperature. Geophys. Res. Lett. 23 (6), 665–668.
Jiang, W., Guo, Z., Sun, X., Wu, H., Chu, G., Yuan, B., Hatte, C., Guiot, J., 2006. Reconstruction of climate and vegetation changes of Lake Bayanchagan (Inner Mongolia): Holocene variability of the East Asian monsoon. Quat. Res. 65 (3), 411–420.
Jiang, Q., Ji, J., Shen, J., Matsumoto, R., Tong, G., Qian, P., Ren, X., Yan, D., 2013. Holocene vegetational and climatic variation in westerly-dominated areas of Central Asia inferred from the Sayram Lake in northern Xinjiang, China. Sci. China-Earth Sci. 56 (3), 339–353.
Kutzbach, J.E., Chen, G., Cheng, H., Edwards, R.L., Liu, Z., 2014. Potential role of winter rainfall in explaining increased moisture in the Mediterranean and Middle East during periods of maximum orbitally-forced insolation seasonality. Clim. Dyn. 42, 1079–1095.
Lavrenko, E.M., Iunatov, A.A., Aleksandr, A., Dashniam, B., 1979. Vegetation Map of Mongolian People's Republic (Scale 1: 1,500,000) Moscow (in Russian). GUGK, Moscow.
Li, J., 1991. Climate of Xinjiang. Meteorological Press, Beijing.
Li, X., Zhao, K., Dodson, J., Zhou, X., 2011. Moisture dynamics in central Asia for the last 15 kyr: new evidence from Yili Valley, Xinjiang, NW China. Quat. Sci. Rev. 30 (23/24), 3457–3466.
Liu, X.Q., Herzschuh, U., Shen, J., Jiang, Q., Xiao, X., 2008. Holocene environmental and climatic changes inferred from Wulungu Lake in northern Xinjiang, China. Quat. Res. 70, 412–425.
Long, H., Shen, J., Chen, J., Tsukamoto, S., Yang, L., Cheng, H., Frechen, M., 2017. Holocene moisture variations over the arid central Asia revealed by a comprehensive sand-dune record from the central Tian Shan, NW China. Quat. Sci. Rev. 174, 13–32.
Luo, D., Xiao, Y., Yao, Y., Dai, A., Ian, S., Christian, L.E.F., 2016. Impact of ural blocking on winter warm Arctic-cold Eurasian Anomalies. Part I: blocking-induced amplification. J. Clim. 29, 3925–3947.
Magny, M., Guiot, J., Schoellammer, P., 2001. Quantitative reconstruction of Younger Dryas to mid-Holocene paleoclimates at Le Locle, Swiss Jura, using pollen and lake-level data. Quat. Res. 56 (2), 170–180.
Magny, M., Begeot, C., Guiot, J., Peyron, O., 2003. Contrasting patterns of hydrological changes in Europe in response to Holocene climate cooling phases. Quat. Sci. Rev. 22 (15–17), 1589–1596.
Marcott, S., Shakun, J., Clark, P., Mix, A., 2013. A reconstruction of regional and global temperature for the past 11,300 years. Science 339 (6124), 1198–1201.
Mathis, M., Sorrel, P., Klotz, S., Huang, X., Oberhansli, H., 2014. Regional vegetation patterns at lake Son Kul reveal Holocene climatic variability in central Tien Shan (Kyrgyzstan, Central Asia). Quat. Sci. Rev. 89, 169–185.
Meeker, L.D., Mayewski, P.A., 2002. A 1400-year high-resolution record of atmospheric circulation over the North Atlantic and Asia. Holocene 12, 257–266.
Nagashima, K., Tada, R., Tani, A., Sun, Y., Isozaki, Y., Toyoda, S., Hasegawa, H., 2011. Millennial-scale oscillations of the westerly jet path during the last glacial period. J. Asian Earth Sci. 40 (6), 1214–1220.
Nakagawa, T., Tarasova, P., Nishida, K., Gotanda, K., Yasuda, Y., 2002. Quantitative pollen-based climate reconstruction in central Japan: application to surface and Late Quaternary spectra. Quat. Sci. Rev. 21 (18–19), 2099–2113.
Niemeyer, B., Klemm, J., Pestryakova, L.A., Herzschuh, U., 2015. Relative pollen productivity estimates for common taxa of the northern Siberian Arctic. Rev. Palaeobot. Palynol. 221, 71–82.
Overpeck, J., Webb, T., Prentice, I., 1985. Quantitative interpretation of fossil pollen spectra- dissimilarity coefficients and the method of modern analogs. Quat. Res. 23 (1), 87–108.
Prentice, I., Cramer, W., Harrison, S., Leemans, R., Monserud, R., Solomon, A., 1992. A global Biome model based on plant physiology and dominance, soil properties and climate. J. Biogeogr. 19 (2), 117–134.
Prentice, I., Guiot, J., Huntley, B., Jolly, D., Cheddadi, R., 1996. Reconstructing biomes from palaeoecological data: a general method and its application to European pollen data at 0 and 6 ka. Clim. Dyn. 12 (3), 185–194.
Prokopenko, A., Khursevich, G., Bezrukova, E., Kuzmin, M., Boes, X., Williams, D., Fedenya, S., Kulagina, N., Letunova, P., Abzaeva, A., 2007. Paleoenvironmental proxy records from Lake Hovsgol, Mongolia, and a synthesis of Holocene climate change in the Lake Baikal watershed. Quat. Res. 68 (1), 2–17.
Ran, M., Feng, Z., 2013. Holocene moisture variations across China and driving mechanisms: a synthesis of climatic records. Quat. Int. 313, 179–193.
Ran, M., Zhang, C., Feng, Z., 2015. Climatic and hydrological variations during the past 8000 years in northern Xinjiang of China and the associated mechanisms. Quat. Int. 358, 21–34.
Reimer, P., Baillie, M., Bard, E., Bayliss, A., Beck, J., Blackwell, P., Ramsey, C., Buck, C., Burr, G., Edwards, R., Friedrich, M., Grootes, P., Guilderson, T., Hajdas, I., Heaton, T., Hogg, A., Hughen, K., Kaiser, K., Kromer, B., McCormac, F., Manning, S., Reimer, R., Richards, D., Southon, J., Talamo, S., Turney, C., van der Plicht, J., Weyhenmeye, C., 2009. INTCAL09 and MARINE09 radiocarbon age calibration curves. Radiocarbon 51 (4), 1111–1150.
Renssen, H., Seppä, H., Heiri, O., Roche, D.M., Goosse, H., Fichefet, T., 2009. The spatial and temporal complexity of the Holocene thermal maximum. Nat. Geosci. 2 (6), 411.
Renssen, H., Seppä, H., Crosta, X., Goosse, H., Roche, D.M., 2012. Global characterization

of the Holocene thermal maximum. Quat. Sci. Rev. 48, 7–19.
Rudaya, N., Tarasov, P., Dorofeyuk, N., Solovieva, N., Kalugin, I., Andreev, A., Daryin, A., Diekmann, B., Riedel, F., Tserendash, N., Wagner, M., 2009. Holocene environments and climate in the Mongolian Altai reconstructed from the Hoton-Nur pollen and diatom records: a step towards better understanding climate dynamics in Central Asia. Quat. Sci. Rev. 28, 540–554.
Seppä, H., Bennett, K.D., 2003. Quaternary pollen analysis: recent progress in palaeoecology and palaeoclimatology. Prog. Phys. Geogr. 27 (4), 548–579.
Shi, P., Körner, C., Hoch, G., 2008. A test of the growth–limitation theory for alpine tree line formation in evergreen and deciduous taxa of the eastern Himalayas. Funct. Ecol. 22 (2), 213–220.
Sjögren, P., van der Knaap, W.O., Huusko, A., van Leeuwen, J.F.N., 2008. Pollen productivity, dispersal, and correction factors for major tree taxa in the Swiss Alps based on pollen-trap results. Rev. Palaeobot. Palynol. 152, 200–210.
Sun, C., Li, J.P., Zhao, S., 2015. Remote influence of Atlantic multidecadal variability on Siberian warm season precipitation. Sci. Rep. 5, 16853.
Syed, F., Giorgi, F., Pal, J., King, M., 2006. Effect of remote forcings on the winter precipitation of central southwest Asia part 1: observations. Theor. Appl. Climatol. 86 (1–4), 147–160.
Tang, Y., 2014. Holocene Environment Change Inferred from the GDGTs from the Peatland in Altai Mountains, Xinjiang. Lanzhou University, Lanzhou, China.
Tarasov, P., Webb, T., Andreev, A., Afanas'eva, N., Berezina, N., Bezusko, L., Blyakharchuk, T., Bolikhovskaya, N., Cheddadi, R., Chernavskaya, M., Chernova, G., Dorofeyuk, N., Dirksen, V., Elina, G., Filimonova, L., Glebov, F., Guiot, J., Gunova, V., Harrison, S., Jolly, D., Khomutova, V., Kvavadze, E., Osipova, I., Panova, N., Prentice, I., Saarse, L., Sevastyanov, D., Volkova, V., Zernitskaya, V., 1998. Present-day and mid-Holocene biomes reconstructed from pollen and plant macrofossil data from the former Soviet Union and Mongolia. J. Biogeogr. 25 (6), 1029–1053.
Tarasov, P., Dorofeyuk, N., Tseva, E.M., 2000. Holocene vegetation and climate changes in Hoton-Nur basin, northwest Mongolia. Boreas 29 204–204.
Wang, W., Feng, Z.D., 2013. Holocene moisture evolution across the Mongolian Plateau and its surrounding areas: a synthesis of climatic records. Earth-Sci. Rev. 122, 38–57.
Wang, F., Qian, N.F., Zhang, Y.L., Yang, H.Q., 1995. Pollen Flora of China. Science Press, Beijing.
Wirth, S., Glur, L., Gilli, A., Anselmetti, F., 2013. Holocene flood frequency across the Central Alps-solar forcing and evidence for variations in North Atlantic atmospheric circulation. Quat. Sci. Rev. 80, 112–128.
Xu, T., Shi, Z., Wang, H., An, Z., 2016. Nonstationary impact of the winter North Atlantic Oscillation and the response of mid-latitude Eurasian climate. Theor. Appl. Climat. 124 (1–2), 1–14.
Yang, Y.P., Zhang, D.L., Lan, B., Feng, Z.D., 2019. Peat $\delta^{13}C_{cellulose}$-signified moisture variations over the past ~2200 years inthe southern Altai Mountains, northwestern China. J. Asian Earth Sci. 174, 59–67.
Yu, G., Prentice, I., Harrison, S., Sun, X., 1998. Pollen-based biome reconstructions for China at 0 and 6000 years. J. Biogeogr. 25 (6), 1055–1069.
Yu, G., Chen, X.D., Ni, J., Cheddadi, R., Guiot, J., Han, H., Li, S., 2000. Palaeovegetation of China: a pollen data-based synthesis for the mid-Holocene and last glacial maximum. J. Biogeogr. 27, 635–664.
Yuan, G.Y., 1986. Vertical vegetation belt of the west area of Altai Mountains. Acta Geograph. Sin. 41 (1), 32–40.
Zhang, D.L., Feng, Z.D., 2018. Holocene climate variations in the Altai Mountains and the surrounding areas: a synthesis of pollen records. Earth-Sci. Rev. 185, 847–869.
Zhang, J.B., Shi, Y.Z., 2002. Research on Climate Change and Short-Term Forecasting in Xinjiang. China Meteorological Press, Beijing.
Zhang, Y., Meyers, P., Liu, X., Wang, G., Ma, X., Li, X., Yuan, Y., Wen, B., 2016. Holocene climate changes in the central Asia mountain region inferred from a peat sequence from the Altai Mountains, Xinjiang, northwestern China. Quat. Sci. Rev. 152, 19–30.
Zhang, D.L., Feng, Z.D., Yang, Y.P., Lan, B., Ran, M., Mu, G., 2018a. Peat $\delta^{13}C_{cellulose}$-recorded wetting trend during the past 8000 years in the southern Altai Mountains, northern Xinjiang, NW China. J. Asian Earth Sci. 156, 174–179.
Zhang, D.L., Yang, Y.P., Lan, B., 2018b. Climate variability in the northern and southern Altai Mountains during the past 50 years. Sci. Rep. 8 (1), 3238.
Zhao, J.J., An, C.B., Huang, Y., Morrill, C., Chen, F.H., 2017. Contrasting early Holocene temperature variations between monsoonal East Asia and westerly dominated Central Asia. Quat. Sci. Rev. 178, 14–23.